Laser-induced asymmetric faceting and growth of a nano-protrusion on a tungsten tip

Hirofumi Yanagisawa, Vahur Zadin, Karsten Kunze, Christian Hafner, Alvo Aabloo, Dong Eon Kim, Matthias F. Kling, Flyura Djurabekova, Jürg Osterwalder, and Walter Wuensch

Citation: APL Photonics **1**, 091305 (2016); doi: 10.1063/1.4967494
View online: http://dx.doi.org/10.1063/1.4967494
View Table of Contents: http://aip.scitation.org/toc/app/1/9
Published by the American Institute of Physics

Laser-induced asymmetric faceting and growth of a nano-protrusion on a tungsten tip

Hirofumi Yanagisawa,[1,2,3,a] Vahur Zadin,[4,5] Karsten Kunze,[6] Christian Hafner,[7] Alvo Aabloo,[4] Dong Eon Kim,[3,8] Matthias F. Kling,[2,9] Flyura Djurabekova,[5] Jürg Osterwalder,[10] and Walter Wuensch[11]

[1]*Institute for Quantum Electronics, ETH Zürich, CH-8093 Zürich, Switzerland*
[2]*Max Planck Institute for Quantum Optics, D-85748 Garching, Germany*
[3]*Max Planck POSTECH/KOREA Res. Init., Pohang, Gyeongbuk 37673, Republic of Korea*
[4]*Intelligent Materials and Systems Lab, Institute of Technology, University of Tartu, Nooruse 1, 50411 Tartu, Estonia*
[5]*Helsinki Institute of Physics and Department of Physics, University of Helsinki, P.O. Box 43, 00014 Helsinki, Finland*
[6]*Scientific Center for Optical and Electron Microscopy, ETH Zürich, CH-8093 Zürich, Switzerland*
[7]*Laboratory for Electromagnetic Fields and Microwave Electronics, CH-8092 Zürich, Switzerland*
[8]*Department of Physics, Center for Attosecond Science and Technology, Pohang University of Science and Technology, Pohang, Gyeongbuk 37673, Republic of Korea*
[9]*Physics Department, Ludwig-Maximilians-Universität München, D-85748 Garching, Germany*
[10]*Physik Institut, Universität Zürich, Winterthurerstrasse 190, CH-8057 Zürich, Switzerland*
[11]*European Organization for Nuclear Research, CERN, 1211 Geneva 23, Switzerland*

(Received 29 July 2016; accepted 30 October 2016; published online 16 November 2016)

Irradiation of a sharp tungsten tip by a femtosecond laser and exposed to a strong DC electric field led to reproducible surface modifications. By a combination of field emission microscopy and scanning electron microscopy, we observed asymmetric surface faceting with sub-ten nanometer high steps. The presence of faceted features mainly on the laser-exposed side implies that the surface modification was driven by a laser-induced transient temperature rise on a scale of a couple of picoseconds in the tungsten tip apex. Moreover, we identified the formation of a nano-tip a few nanometers high located at one of the corners of a faceted plateau. The results of simulations emulating the experimental conditions are consistent with the experimental observations. The presented technique would be a new method to fabricate a nano-tip especially for generating coherent electron pulses. The features may also help to explain the origin of enhanced field emission, which leads to vacuum arcs, in high electric field devices such as radio-frequency particle accelerators. [http://dx.doi.org/10.1063/1.4967494]

A metallic nano-tip with sharpness of a few nanometers, or even atomic level, can provide very bright and spatially coherent electron waves.[1–5] This is highly beneficial in many applications such as electron diffraction, microscopy, and holography.[6–8] During irradiation by laser pulses a nano-tip is also expected to generate pulsed electron waves with high brightness and coherence.[9–13] Such electron pulses enable experiments with high temporal and spatial resolution for investigations of ultrafast phenomena in solids.[14] A high-performance pulsed electron source would significantly enhance the capability of modern ultrafast devices.[15]

Various well-established methods have been used to fabricate nano-tips.[1–4,16–19] Typically, a nano-tip is grown on a larger metallic tip by applying strong DC fields,[2–4,16–18] heating,[3,17,18] or

[a]Electronic mail: hirofumi.yanagisawa@mpq.mpg.de

depositing metal.[1,4] Fabrication of a nano-tip *in situ* for laser-induced electron pulse applications is, however, not a simple task because of the presence of optical elements used in the laser focusing system which must remain very clean. A nanostructure can also be built up simply by adsorbate molecules attached to clean surfaces of the tips with strong DC fields,[19] but the necessity of residual molecules reduces the controllability of the growth process and the sustainability of the nano-tip under laser irradiation would be questionable. If the formation of a nano-tip can be driven by the laser itself, this will simplify and enhance the nano-tip fabrication process.

So far only indications of surface modification on a nanometer scale, formed under strong AC electric fields, have been reported. For instance, periodic nanostructures were formed on a surface through the excitation of surface plasmons following femtosecond laser ablation[20] and also asymmetric surface modification at an apex of a metal tip was formed by laser asymmetric heating.[21–24] In atom probe tomography experiments, atom migration followed by surface detachment due to bond-breaking and ionization by very high electric fields can be observed.[25–27] However, the formation of a stable surface nano-tip growing on the surface due to irradiation of laser has not been reported in these studies.[20–26] On the other hand, applying strong electric fields on the metal surface by radio-frequency electromagnetic waves, strongly enhanced field emission currents often are measured from macroscopic surfaces, which implies a local electric field enhancement due to the formation of nanostructures.[28–31] A theoretical study suggests the formation of nano-protrusions,[32] but experimental efforts to identify the features responsible for enhanced field emission by using electron microscopy have been unsuccessful, given the inherent difficulty of identifying nano-scale features on centimeter-sized surfaces and correlating with field emission measured centimeters away.

Here we have found that laser radiation can indeed induce a nano-tip. By using field emission microscopy (FEM) and high-resolution scanning electron microscopy (SEM) and performing local field simulations for the observed structures, we have investigated laser-induced surface modification of a tungsten tip apex. We have observed that faceting with sub-10 nm steps was induced asymmetrically on the tip apex and a nano-protrusion was grown at one corner of the step edges by a combination of illuminating femtosecond laser pulses and applying strong DC fields.

Applying high voltages on a metallic tip with nanometer sharpness resulted in a field concentration only at the tip apex and the strong field drives field emission (FE) via electron tunneling through the surface barrier.[33] The FE current exponentially depends on the work function and local fields on the tip apex.[33] Thereby FEM provides geometrical information on the tip apex and can achieve a spatial resolution of 1 or 2 nm. The FEM experiments were performed in an ultra-high vacuum chamber (base pressure: $1 \cdot 10^{-10}$ mbar). A phosphor screen with a Chevron-type double-channelplate amplifier in front of the tip is used to record the FE patterns. All the measurements were done at room temperature.

In our experiments, we used a single crystal tungsten tip with the tip apex orientated in the (011) direction. A clean tip apex can be obtained by heating the tip.[33,34] With increasing heating temperature, the radius of curvature becomes bigger; the radius of curvature was approximately 250 nm in this study. When the tip apex is clean, FEM images show a characteristic pattern such as the one in Fig. 1(a). In this pattern, the intensity distribution roughly represents the work function map because the local-field distribution changes moderately over the tip apex. Here the most intense emission spots seen in Fig. 1(a) correspond to the (310) crystal faces with the lowest work function. On the other hand, an increase of field emission currents can be due to the local field enhancement caused by geometric nanofeatures formed on the tip apex. The appearance of laser-induced nanofeatures described in this letter was recorded via this mechanism.

The cleaned tip was subject to pulsed laser irradiation with a laser power of 180 mW. Laser pulses are generated in a Ti:sapphire oscillator (center wavelength: 830 nm; repetition rate: 80 MHz; pulse width: sub-10 fs) and introduced into the vacuum chamber. The laser was focused on to the tip apex by a parabolic lens (focal length: $f = 15$ mm); the diameter of the focused beam is approximately 3.5 μm ($1/e^2$ radius). Linearly polarized laser light was used with the polarization vector parallel to the tip axis. During the laser irradiation, a DC voltage of −3000 V was applied to the tip. Periodically, we paused the laser irradiation and recorded FEM images. The exposure time for the FEM images was 2.5 s. The tip voltages were set manually in each case to provide sufficiently strong electron signals on the FEM fluorescent screen but avoiding saturation of the signal.

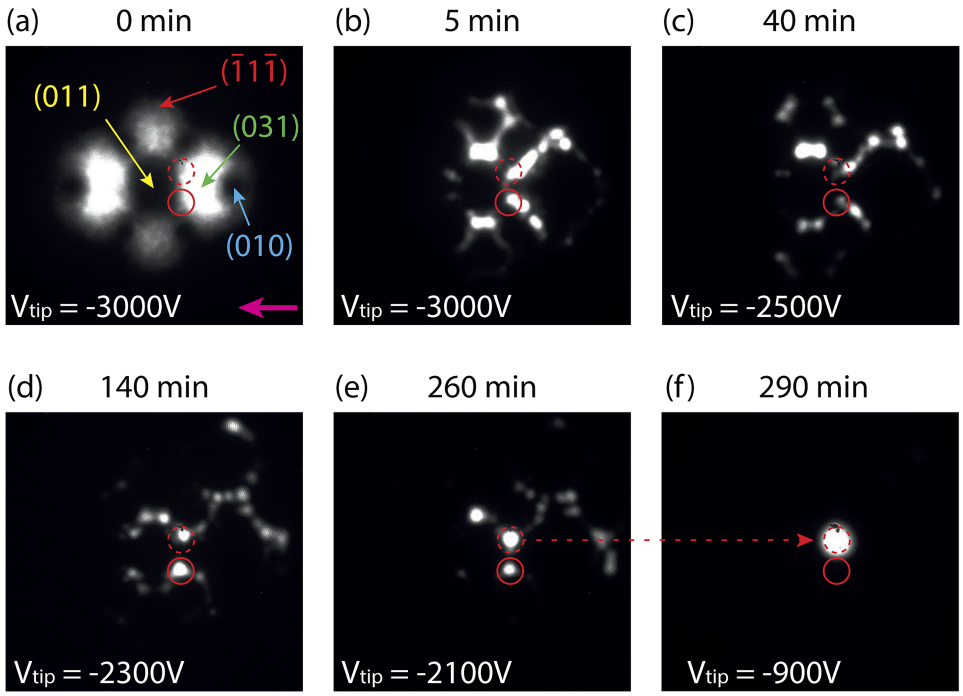

FIG. 1. ((a)–(f)) Field emission patterns without laser some time after laser irradiation. During the laser irradiation, V_{tip} was −3000 V and *PL* was 180 mW. The propagation direction of the laser is indicated by a pink arrow in (a). Tip voltages and accumulated irradiation time are shown on each corresponding image. (a) is the pattern from the tip apex cleaned by flash heating prior to irradiation. Here, the surface indices of some facets are also indicated. Two red circles are placed in all the panels as makers of locations of bright spots appeared in (e).

Figure 1 shows the evolution of the FE patterns which we observed during the experiment for a laser irradiation time which was approximately 5 h. The time displayed in each figure is the accumulated laser irradiation time. As one can see, already after the first 5 min of laser irradiation, the emission pattern had changed significantly from the original one. The extended bright areas in the original FE pattern from the faces with the low work function were replaced by dotted-line features, which appeared asymmetrically, mainly on the laser-exposed side. During laser irradiation, the vacuum in the chamber was maintained at a pressure below $3 \cdot 10^{-10}$ mbar. Normally, FEM images do not change significantly due to the absorption of contaminants if the tip is left in such a vacuum condition for less than 5 min without laser irradiation (see the supplementary material). In addition, a DC electric field alone does not produce an asymmetric pattern during FEM experiments.[2,21] Therefore, the change of the FEM images appears to have been induced by the laser. As will be discussed later, these features form as a consequence of the step edges of faceted surfaces where local fields are enhanced.

The dotted line structures remained stable until Fig. 1(e), while tip voltage decreases gradually with irradiation time, implying the increase of field enhancement factors due to the formation of smaller nano-structures.[16,17] After some irradiation time, intense emission spots can be seen in the FEM images such as Figs. 1(d) and 1(e). Two bright spots are especially intense and are marked by red circles. Their relative intensities change from image to image. At 290 min in Fig. 1(f), a bright spot suddenly appeared in the position of the upper intense spot. For this condition the tip voltage had to be significantly lowered, to maintain the level of image quality and avoid the saturation of the detector. The appearance of the bright spot and the strong reduction of the tip voltage indicate the formation of a nano-tip.[16,17] It should be mentioned that the laser-induced changes in FEM are repeatable. By heating the sample, the sample condition can be set back to the original clean condition and FE pattern of Fig. 2(a) can be observed, and similar FEM images can be obtained again after laser irradiation. Note that we produced nano-tips twice by the present method on different tips.

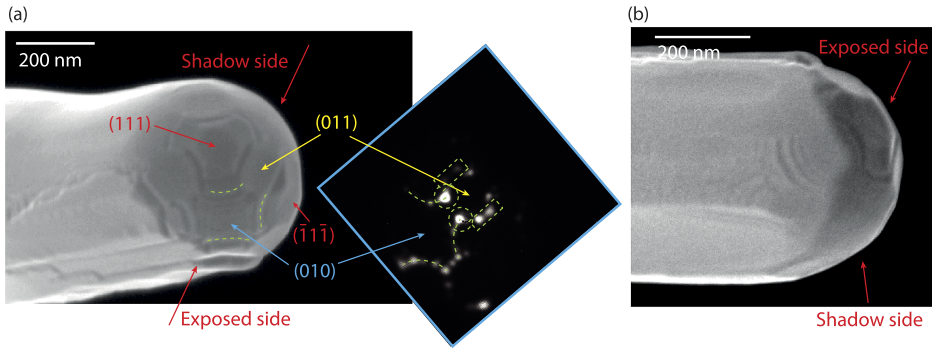

FIG. 2. ((a) and (b)) SEM images of the tungsten tip apex with a nano-tip from different view points, acquired in the high resolution (immersion) mode using the secondary electron detector (through-the-lens detector) at 2 kV and a working distance of 4 mm. The white scale bars indicating 200 nm. The inset of (a) is the electron emission pattern identical to Fig. 1(d).

In order to investigate the origin of the dotted-line structures and the bright spot, we removed the sample from the vacuum chamber and inspected the tip apex with a high-resolution SEM (FEI Magellan).[35] Figs. 2(a) and 2(b) show SEM images of the tip apex from two different view points, the laser-exposed and the shadow sides. From these two viewing perspectives, the asymmetric surface restructuring on the tip apex can be seen. Faceting was mainly observed on the exposed side, including the shank, as shown in Fig. 2(a). The surface on the shadow side, by contrast, remained rather smooth as it is shown in Fig. 2(b). Note that some laser-induced surface modifications on tip apexes were observed in previous work,[21–23] but not the gradual growth of prominent features, which we observed in our experiments have been reported so far.

Comparing the SEM with FEM in the inset of Fig. 2(a), very similar curved structures were found on the exposed side as indicated by dashed green curves. From the similarity in symmetry and shape, we deduce that the electrons were emitted from these curved features outlining the facet with the (010) crystal face. Other faces can be identified based on the symmetries and relative position with respect to the (010) surface as shown in Fig. 2(a).

To clarify the origin of the surface features observed in the SEM images, the SEM images were taken from several view points, View A–D, as indicated in Fig. 3(a). The line structures, especially those indicated in Fig. 3 as Step1 and Step2, were clearly resolved as steps with a height of approximately 8 nm in the side-view (View A in Fig. 3(b)). In the same image, the facets of (011) and (111) orientations are also clearly observed as indicated by yellow and red lines, respectively. The angles between yellow and red lines are approximately 35°, which agrees with the theoretical value of the angle between (011) and (111) crystallographic planes in the tungsten lattice. The available view of the (010) surface makes it more difficult to determine if there are steps, however it is likely that there are, in analogy with those clearly seen on the (011) surface. Indeed there is some indication that there may even be more steps, and candidates are marked by blue lines in Fig. 3(c).

The facets which have been formed intersect with each other and form ridges as indicated by a dashed line in Figs. 3(a) and 3(c). In addition, there are corners where (011), (111), and (010) facets are intersected as marked by green dashed circles in Fig. 3(a). The ridges and corners have sharper edges so that the corresponding local fields are higher than at other places on the tip apex. Indeed, the spots seen in the FEM images which form curved lines around (010) in the inset of Fig. 2(a) appear to lie on the ridges surrounding the (010) facet. The other field emission spots, marked by rectangles and circles in the inset, can be consistently explained by ridges and corners, respectively. Now most importantly, a nano-tip appears to have grown at one of the corners as indicated by a black arrow in Fig. 3(a). In fact, we have observed a faint feature of a nano-protrusion protruding from the corner as denoted by the green arrow in Figs. 3(d)–3(f). In order to emphasize the feature, the red dashed lines are drawn to show outlines in Figs. 3(e) and 3(f). The height of the observed nano-tip is estimated to be approximately 3 nm. It should be mentioned that similar but larger nano-protrusions were grown by applying strong DC fields with elevated temperature in previous work.[16]

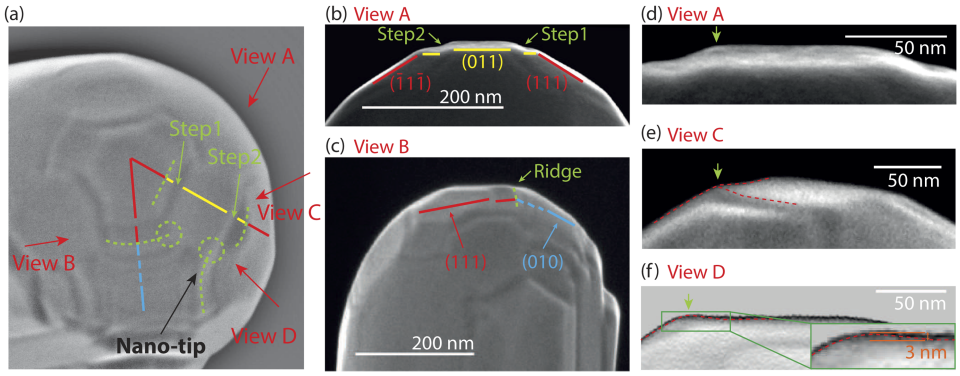

FIG. 3. ((a)–(f)) SEM images of the tungsten tip apex from different view points and for different magnifications. In all images, the yellow, red, and blue lines indicate (011), (111), and (010) type facets, respectively. The dashed lines and circles indicate ridges and corners, respectively, formed by the intersection of facets. (a) shows only the apex of the tip from the same image as in Fig. 2(a). Edges of structures observed in (a) and (f) are intensified for more clear visualization. The different view points of imaging the tip apex shown in (b)–(f) are roughly indicated as Views A–D. The white scale bars are 200 nm in (b) and (c) and 50 nm in (d)–(f). The green arrow indicates the location of the nano-tip in (d)–(f).

The identification of this feature in the SEM as a nano-protrusion is supported by simulations of field enhancement effects. The changes of the enhancement factors in experiments can be approximately estimated from the threshold voltages where the FE current reaches an observable level by the two-dimensional electron detector in our experimental setup. The threshold voltages for the sample conditions in Figs. 1(a), 1(e), and 1(f) were 2500 V, 1800 V, and 700 V, respectively. The applied voltage V can be converted to a local field at the tip apex F_L via $F_L = C_L V$, where C_L is the voltage conversion factor (VCF). Here, assuming that the local fields are the same at the threshold voltages, we can calculate the change in the VCFs, which should correspond to the change of field enhancement factors. The VCFs change by a factor of 1.39 from the sample conditions of Figs. 1(a)–1(e) and by factor of 2.57 from Figs. 1(e) and 1(f). The errors of these values are determined from the resolution of the voltage measurements and the intensity resolution of the screen (See the supplementary material).

We have performed the simulations of local field distributions and determined changes of field enhancement factors simply by the ratio of the local maximal fields for three different geometries as shown in Figs. 4(a)–4(c). The geometries were set to match the above-mentioned experimental observations. Three geometries can be described as follows. The first (Fig. 4(a)) is a perfect hemispherical shape with a radius of curvature of 250 nm to represent the as-prepared tip apex. The second has a rectangular plateau on the tip apex as shown in Fig. 4(b). The plateau is surrounded by the steps and sharp corners to represent the (011) facet seen in Fig. 3(b). We modeled this structure since the field emission current in the experiment was the strongest at one of the corners of such a plateau (cf. Fig. 2(a)) and the dimensions of the rectangular plateau in the model were the same as in the SEM observation in Figs. 3(d) and 3(f). The third is shown in Fig. 4(c) and has a nano-hemisphere with the radius of 3 nm (see Fig. 3(f)) placed at one of the corners of the plateau, where the local fields caused by the plateau are at a maximum, as shown in Fig. 4(b).

The simulations of local DC fields were performed by using Comsol Multiphysics.[36] Assuming no space charge density in vacuum around the tip, the electric field distribution was obtained by solving the Laplace equation for the defined geometries[37] (see the supplementary material for details). In the simulations, the applied field was the same for all three geometries, which was along with the center axis of the tip apex, and was chosen to result in the maximum field F_1 = 2 V/nm for the hemispherical tip as shown in Fig. 4(a). This is a typical field strength which results in field emission from a tungsten tip.[12] The field enhancement factor of the hemisphere was 3, which is consistent with the analytical value.[38] Comparing now the ratios of the maximal local fields in all three geometries, we observe a gradual enhancement of the local fields very similar to that measured in the experiment. Indeed, the value of the maximal local field from Fig. 4(a) (F_1) to 4b (F_2) changed by F_2/F_1 = 1.37 (compared to 1.39 measured in the experiment) and from Fig. 4(b) (F_2) to 4c (F_3) by factor F_2/F_1 = 2.48 (compared to 2.57 in the experiment).

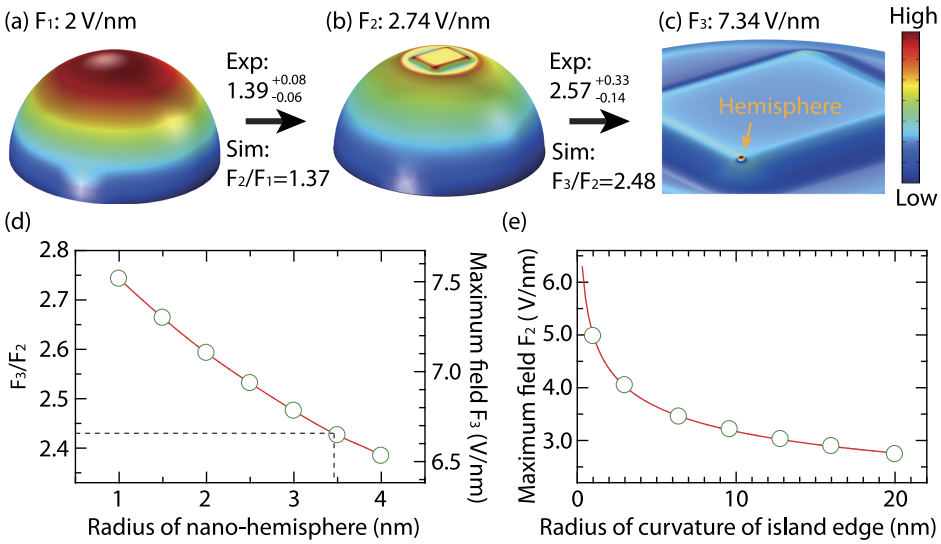

FIG. 4. ((a)–(c)) Local field distributions on a tip apex with different shapes. (a) Hemispherical tip apex, (b) hemispherical tip with a rectangular plateau on top of the apex, and (c) nano-hemisphere at one corner of the rectangular plateau of (b). See the text for details. Maximum local fields for the three models, $F1$, $F2$, and $F3$, are shown in each figure. (d) Changes of maximum fields with varying radius of the nano-hemisphere. The maximum fields are shown on the right side axis. The left side axis shows changes of field enhancement factors with respect to that of (b). (e) Changes of maximum fields with varying radius of curvature of the plateau in (b).

The observed size of the nano-tip is also supported by further field distribution simulations. By varying the radius of the nano-hemisphere, we analyzed the evolution of the factor F_3/F_2. As can be seen in Fig. 4(d), the enhancement of the local field meets the experimental value 2.57 [+0.33, −0.14] if the radius of the nano-hemisphere is smaller than 3.5 nm (the dashed lines in Fig. 4(d) indicate the lower boundary as a guide for the eye). This result is consistent with our SEM observation within its experimental errors.

A pyramidal shape of a surface feature obtained by an intersection of three facets was also simulated to check if such a feature alone could cause the observed field enhancement. This could be due to a strong local enhancement due to the atomic level sharpness of the top of the pyramid.[16–18] As can be seen in Fig. 4(e), the simulations did not confirm this hypothesis. Sharpening the pyramidal top appeared to be insufficient to account for the observed field enhancement. Even a curvature radius of 0.3 nm (interatomic distance of the tungsten lattice) of the simulated plateau corner did not result in a sufficiently high local field. Note that a previous study showed that local field variation for an atomically sharp step edge is only a factor of around 2, not much greater.[39] Hence all the observations and simulations coherently support the presence of a nano-tip at a corner of the surface facets with the well pronounced surrounding steps.

It is known that applying a strong DC bias on a heated tip drives faceting on the tip apex.[16–18,40] Although we do not heat our sample during the experiment, the laser pulses irradiating the tip apex cause local heating, which in combination with the strong electric field leads to the surface modification. Heating of the crystal lattice occurs through energy absorption from the laser pulses by electrons and the subsequent energy transfer from the excited electrons to the lattice. Although the elevated lattice temperature lasts up to nanoseconds after each laser pulse, the temperature rises quite high during the first 10 ps after laser excitation. More importantly, within a couple of picoseconds after laser excitation, the temperature distribution is very asymmetric with higher temperatures on the laser-exposed side.[41] After the first period of a hot and asymmetric temperature distribution, the temperature significantly decreases and the distribution becomes uniform. Therefore, the observed asymmetric faceting on the exposed side must be driven by the transient thermal effects on a time scale of a couple of picoseconds. Our assessment of this time span, for instance, coincides with the interval of atom evaporation after interaction with ultrafast lasers that was observed in previous laser-assisted atom probe tomography experiments (30 ± 20 ps).[42] For the nano-tip, it appears that

its growth requires the stronger electric fields caused by the facet edge because of its location there. Hence, the laser-induced faceting is the essential initial step which then results in the growth of a nano-protrusion. Since the surface energy minimization principle suggests that small nano-protrusions on a flat surface would tend to collapse,[43] we believe that this is an important conclusion.

In summary, we have observed asymmetric faceting and growth of a nano-protrusion on a tungsten tip apex induced by a combination of sub-ten femtosecond laser pulses and strong DC fields. This is a new method to create a nano-tip and can likely be also used for processing nano-patterns on the sub-ten nanometer scale by faceting. The growth of nano-tips under intense fields is also of potential importance to the particle accelerator community. A strong rf-field may induce the nano-tip growth on the surfaces of rf cavities in the same way as on the tip. Vacuum arcing, initiated from enhanced field emission, limits the strength of the rf-fields and thus the achievable accelerating gradient.[28] As it was shown in Ref. 19, the growth of nano-protrusions under strong DC electric fields leads to vacuum arcing. This is why the investigation of the formation of nano-tips under intense electric fields may be an important input for finding technological solutions for increasing the gradient in normal conducting radiofrequency accelerating structures. It is, moreover, very difficult to observe a tip of a few nanometers size grown on a macroscopic surface of the cavity surface. Hence the laser-induced surface modification on the tip presented in this work has the potential to become an excellent research tool for investigating and understanding the growth mechanism of surface nano-features under extreme conditions.

See the supplementary material for (1) changes of FEM images with time, (2) estimation of errors of the observed changes in the voltage conversion factors, and (3) details of local DC field simulations.

This work was supported by the Swiss National Science Foundation through the Ambizione (Grant No. PZ00P2_131701) and the NCCR MUST, Kazato Research Foundation, Estonian Science Foundation Grant No. PUT 57, the Academy of Finland (Grant No. 296969), the National Research Foundation of Korea through Global Research Laboratory Program (Grant No. 2009-00439) and Max Planck POSTECH/KOREA Research Initiative Program (Grant No. 2016K1A4A4A01922028), the DFG via SPP1840 and the EU via the grant ATTOCO (Grant No. 2011-0031558) . We thank Professor C. Oshima and Dr. Lukas Gallmann for fruitful discussions and M. Baer for technical support.

[1] T.-Y. Fu, L.-C. Cheng, C.-H. Nien, and T. T. Tsong, Phys. Rev. B **64**, 113401 (2001).
[2] K. Nagaoka, H. Fujii, K. Matsuda, M. Komaki, Y. Murata, C. Oshima, and T. Sakurai, Appl. Surf. Sci. **182**, 12 (2001).
[3] V. T. Binh and N. García, Ultramicroscopy **42-44**, 80 (1992).
[4] H. W. Fink, IBM J. Res. Dev. **30**, 460 (1986).
[5] C. Oshima, K. Mastuda, T. Kona, Y. Mogami, M. Komaki, Y. Murata, T. Yamashita, T. Kuzumaki, and Y. Horiike, Phys. Rev. Lett. **88**, 038301 (2002).
[6] J. M. Zuo, I. Vartanyants, M. Gao, R. Zhang, and L. A. Nagahara, Science **300**, 1419 (2003).
[7] Z. L. Wang, J. Phys. Chem. B **104**, 1153 (2000).
[8] A. Tonomura, PNAS **102**, 14952 (2005).
[9] M. J. G. Lee, Phys. Rev. Lett. **30**, 1193 (1973).
[10] P. Hommelhoff, Y. Sortais, A. Aghajani-Talesh, and M. A. Kasevich, Phys. Rev. Lett. **96**, 077401 (2006).
[11] H. Yanagisawa, C. Hafner, P. Doná, M. Klöckner, D. Leuenberger, T. Greber, M. Hengsberger, and J. Osterwalder, Phys. Rev. Lett. **103**, 257603 (2009).
[12] H. Yanagisawa, M. Hengsberger, D. Leuenberger, M. Klöckner, C. Hafner, T. Greber, and J. Osterwalder, Phys. Rev. Lett. **107**, 087601 (2011).
[13] M. Schenk, M. Krüger, and P. Hommelhoff, Nature **475**, 78 (2011).
[14] M. Gulde, S. Schweda, G. Storeck, M. Maiti, H. K. Yu, A. M. Wodtke, S. Schäfer, and C. Ropers, Science **345**, 200 (2014).
[15] A. Schiffrin, T. Paasch-Colberg, N. Karpowicz, V. Apalkov, D. Gerster, S. Mühlbrandt, M. Korbman, J. Reichert, M. Schultze, S. Holzner, J. V. Barth, R. Kienberger, R. Ernstorfer, V. S. Yakovlev, M. I. Stockman, and F. Krausz, Nature **493**, 70 (2013).
[16] S. Fujita and H. Shimoyama, Phys. Rev. B **75**, 235431 (2007).
[17] S. Fujita and H. Shimoyama, J. Vac. Sci. Technol. B **26**, 738 (2008).
[18] E. Rokuta, T. Nakagawa, H. Murata, S. Fujita, H. Shimoyama, and C. Oshima, Jpn. J. Appl. Phys. **50**, 115001 (2011).
[19] K. S. Yeong and J. T.L. Thong, J. Appl. Phys. **99**, 104903 (2006).
[20] J. Reif, O. Varlamova, and F. Costache, Appl. Phys. A **92**, 1019 (2008).
[21] A. Shariq, S. Mutas, K. Wedderhoff, C. Klein, H. Hortenbach, S. Teichert, P. Kü cher, and S. S. A. Gerstl, Ultramicroscopy **109**, 472 (2009).
[22] S. Koelling, N. Innocenti, A. Schulze, M. Gilbert, A. K. Kambham, and W. J. Vandervorst, Appl. Phys. **109**, 104909 (2011).
[23] G. Sha, A. Cerezo, and G. D. W. Smith, Appl. Phys. Lett. **92**, 043503 (2008).
[24] A. Vella, Ultramicroscopy **132**, 5 (2013).

[25] B. Gault, F. Danoix, K. Hoummada, D. Mangelinck, and H. Leitner, Ultramicroscopy **112**, 182 (2012).
[26] T. T. Tsong, Prog. Surf. Sci. **67**, 235 (2001).
[27] M. K. Miller and R. G. Forbes, *Atom Probe Tomography: The Local Electrode Atom Probe* (Springer, New York, 2014).
[28] W. Wuensch, CERN-OPEN-2014-028, CLIC-Note-1025, 2014.
[29] A. Grudiev, S. Calatroni, and W. Wuensch, Phys. Rev. Spec. Top.–Accel. Beams **12**, 102001 (2009).
[30] H. Chen, Y. Du, W. Gai, A. Grudiev, J. Hua, W. Huang, J. G. Power, E. E. Wisniewski, W. Wuensch, C. Tang, L. Yan, and Y. You, Phys. Rev. Lett. **109**, 204802 (2012).
[31] A. Degiovanni, W. Wuensch, and G. J. Navarro, Phys. Rev. Accel. Beams **19**, 032001 (2016).
[32] A. S. Pohjonen, S. Parviainen, T. Muranaka, and F. Djurabekova, J. Appl. Phys. **114**, 033519 (2013).
[33] R. Gomer, *Field Emission and Field Ionization*(American Institute of Physics, New York, 1993).
[34] M. Sato, Phys. Rev. Lett. **45**, 1856 (1980).
[35] L. Reimer, *Scanning Electron Microscopy: Physics of Image Formation and Microanalysis*, 2nd ed. (Springer, 1998).
[36] See http://www.comsol.com/ for information about Comsol Multiphysics.
[37] V. Zadin, A. Pohjonen, A. Aabloo, K. Nordlund, and F. Djurabekova, Phys. Rev. Spec. Top.–Accel. Beams **17**, 103501 (2014).
[38] R. G. Forbes, C. J. Edgcombe, and U. Valdré, Ultramicroscopy **95**, 57 (2003).
[39] B. Lepetit, D. Lemoine, and M. Márquez-Mijares, J. Appl. Phys. **120**, 085105 (2016).
[40] L. W. Swanson and G. A. Schwind, "Review of the Zr/O Schottky cathode," in *Handbook of Charged Particle Optics*, 2nd ed., edited by J. Orloff (CRC Press, Baton Rouge, 2009), Chap. 1.
[41] C. Kealhofer, S. M. Foreman, S. Gerlich, and M. A. Kasevich, Phys. Rev. B **86**, 035405 (2012).
[42] F. Vurpillot, J. Houard, A. Vella, and B. Deconihout, J. Phys. D: Appl. Phys. **42**, 125502 (2009).
[43] J. F. M. Rusanen, K. Nordlund, and I. T. Koponen, J. Phys.: Condens. Matter **16**, 2995 (2004).